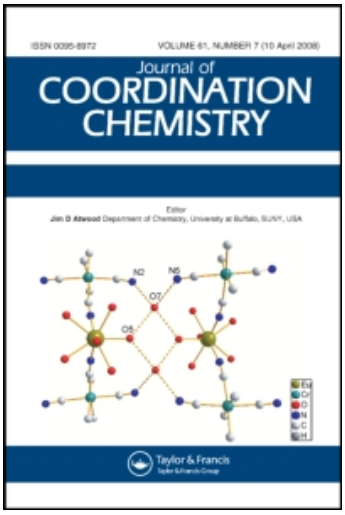

Journal of Coordination Chemistry
Publication details, including instructions for authors and subscription information:
http://www.informaworld.com/smpp/title~content=t713455674

Transition metal complexes of 2-amino-3-chloro-5-trifluoromethylpyridine: syntheses, structures, and magnetic properties of $[(TMCAPH)_2CuBr_4]$ and $[(TMCAPH)_2CuCl_4]$

Jan L. Wikaira[a]; Lixin Li[b]; Ray Butcher[c]; Christopher M. Fitchett[a]; Geoffrey B. Jameson[d]; Christopher P. Landee[e]; Shane G. Telfer[d]; Mark M. Turnbull[b]
[a] Department of Chemistry, University of Canterbury, Christchurch 8041, New Zealand [b] Carlson School of Chemistry and Biochemistry, Clark University, Worcester, MA 01610, USA [c] Department of Chemistry, Howard University, Washington, DC 20059, USA [d] Institute of Fundamental Sciences, Massey University, Palmerston North 4442, New Zealand [e] Department of Physics, Clark University, Worcester, MA 01610, USA

First published on: 28 July 2010

To cite this Article Wikaira, Jan L. , Li, Lixin , Butcher, Ray , Fitchett, Christopher M. , Jameson, Geoffrey B. , Landee, Christopher P. , Telfer, Shane G. and Turnbull, Mark M.(2010) 'Transition metal complexes of 2-amino-3-chloro-5-trifluoromethylpyridine: syntheses, structures, and magnetic properties of $[(TMCAPH)_2CuBr_4]$ and $[(TMCAPH)_2CuCl_4]$', Journal of Coordination Chemistry, 63: 17, 2949 — 2964, First published on: 28 July 2010 (iFirst)
To link to this Article: DOI: 10.1080/00958972.2010.505284
URL: http://dx.doi.org/10.1080/00958972.2010.505284

Journal of Coordination Chemistry
Vol. 63, No. 17, 10 September 2010, 2949–2964

Transition metal complexes of 2-amino-3-chloro-5-trifluoromethylpyridine: syntheses, structures, and magnetic properties of $[(TMCAPH)_2CuBr_4]$ and $[(TMCAPH)_2CuCl_4]$

JAN L. WIKAIRA*†, LIXIN LI‡, RAY BUTCHER¶, CHRISTOPHER M. FITCHETT†, GEOFFREY B. JAMESON⊥, CHRISTOPHER P. LANDEE§, SHANE G. TELFER⊥ and MARK M. TURNBULL‡

†Department of Chemistry, University of Canterbury, PB 4800, Christchurch 8041, New Zealand
‡Carlson School of Chemistry and Biochemistry, Clark University, 950 Main Street, Worcester, MA 01610, USA
§Department of Physics, Clark University, 950 Main Street, Worcester, MA 01610, USA
¶Department of Chemistry, Howard University, 525 College Street, NW, Washington, DC 20059, USA
⊥Institute of Fundamental Sciences, Massey University, PB11222, Palmerston North 4442, New Zealand

(*Received 4 May 2010; in final form 5 May 2010*)

The reaction of CuX_2 (X = Br or Cl) with 2-amino-3-chloro-5-trifluoromethylpyridine in aqueous acids (HX; X = Br or Cl) yields bis(2-amino-3-chloro-5-trifluoromethylpyridinium) tetrabromocuprate(II) (**1**) and bis(2-amino-3-chloro-5-trifluoromethylpyridinium) tetrachlorocuprate(II) (**2**). These compounds have been characterized by IR, powder X-ray diffraction (XRD), single crystal XRD, combustion analysis, and temperature-dependent magnetic susceptibility. Compound **1** crystallizes in the monoclinic space group $P2_1/c$ with three ions in the asymmetric unit, whereas **2** crystallizes in the triclinic space group $P\bar{1}$, and the asymmetric unit contains 18 ionic moieties. Both compounds exhibit antiferromagnetic exchange *via* the double halide exchange pathway and singlet ground states, with stronger exchange observed for **1**. Both compounds exhibit multiple potential magnetic exchange pathways, but fitting of the data to available analytical models suggests that the magnetic exchange constants $2J/k_B$ are ~50 K in **1** and ~6 K in **2**, respectively.

Keywords: 2-Amino-3-chloro-5-trifluoromethylpyridine; Tetrahalocuprates; Crystal structure; Magnetism

1. Introduction

Significant investigation into the propagation and possible mechanisms for magnetic exchange in cuprate salts has led to a variety of pathways having been elucidated [1].

*Corresponding author. Email: jan.wikaira@canterbury.ac.nz

ISSN 0095-8972 print/ISSN 1029-0389 online © 2010 Taylor & Francis
DOI: 10.1080/00958972.2010.505284

One of these, which involves magnetic exchange *via* non-bonding contacts between halide ions attached to a variety of metals [2], has been of particular interest to the authors. This pathway, M–X···X–M, is described as a double halide bridge. The degree of magnetic exchange *via* the double halide bridge in such complexes has been shown to range from weakly antiferromagnetic ($2J/k_B = -1.3(5)$ K) [3] to relatively strong ferromagnetic ($2J/k_B = 250$ K) [4]. In building a library of compounds to facilitate the investigation of the factors controlling the sign and strength of the magnetic exchange through these double halide bridges, a series of compounds with the general formula $A_2[MX_4]$ has been synthesized, where A is an organic cation, M is a 2+ transition metal ion, usually Cu^{2+}, and X either Cl or Br. The organic cations are usually protonated bases, such as alkyl amines [5], substituted pyridines [6], or 2-aminopyrimidine [7].

If it is assumed that the strength of the magnetic exchange is dependent on both the degree of delocalization of spin density from Cu(II) to the halide and the orbital overlap between the two non-bonding halide ions, then a number of variables become apparent. These factors divide into those within the tetrahalocuprate ions and those between the ions. Figure 1 shows the geometric parameters for describing the interaction between two CuX_4^{2-} ions. A proposed system for the interaction topology is fully explained [8]. The distances and angles in these two-halide bridges are determined by the packing of the molecules or ions in the crystal. Changes in the crystal packing can be brought about by changing the size and shape of the cation.

Considerable interest is currently being shown in molecules containing CuX_4^{2-}. Recent examples involving structural and/or magnetic data include bis(3-bromopyridinium)tetrachlorocuprate(II) [9], (−)-sparteinium tetrachlorocuprate(II) monohydrate [10], bis(2-chloropyridinium)tetrachlorocuprate(II) [11], bis(2-amino-5-fluoropyridinium)tetrachlorocuprate(II) [12], bis(1-*n*-butyl-3-methylimidazolium) tetrachlorocuprate(II) [13], bis(1,3,2-benzodithiazolium)tetrachlorocuprate(II) [14], bis(2,3-dimethylpyridinium)tetrabromocuprate(II) [15], 2,5-dibromopyridinium tetrachlorocuprate(II) [16], *bis*(imidazolium)tetrachlorocuprate(II) [17], and bis(2-chloropyridinium)tetrachlorocuprate(II) [18] complexes.

With respect to substituted pyridines, Turnbull *et al*. [19] have previously studied the bis(2-amino-5-S-pyridinium)Cu(II)X_4 [5-SAP] family, where S = Me, Cl, or Br [19a, c] and the bis(3-amino-2-chloropyridinium)-$Cu^{II}X_4$ compounds, where X = Cl or Br. In these families, the crystal packing is affected by the size of the S-substituent and in part dominated by hydrogen-bond donating properties of the 2- or 3-aminopyridinium N–H groups. In this study, using the previously unreported bis(2-amino-3-chloro-5-trifluoromethylpyridinium) cation, the addition of the strongly electron-withdrawing trifluoromethyl group was expected to significantly affect the hydrogen bond donating properties of the cationic species. We report here the synthesis, structure, and magnetic characterization of bis(2-amino-3-chloro-5-trifluoromethylpyridinium)

d – The distance between the X atoms

θ_1 – The angle Cu_1-X_1···X_2

θ_2 – The angle Cu_2-X_2···X_1

τ – The dihedral angle Cu_1–X_1···X_2–Cu_2

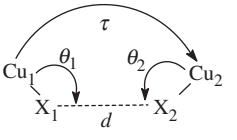

Figure 1. The geometric parameters for describing the interaction between two CuX_4^{2-} ions.

tetrabromocuprate(II), $(TMCAPH)_2[CuBr_4]$ (**1**) and bis(2-amino-3-chloro-5-trifluoromethylpyridinium)tetrachlorocuprate(II), $(TMCAPH)_2[CuCl_4]$ (**2**).

2. Experimental

2.1. *General*

2-Amino-3-chloro-5-trifluoromethylpyridine, hydrochloric acid, and hydrobromic acid were purchased from the Aldrich Chemical Company and used without purification. Copper(II) chloride and copper(II) bromide were obtained from Baker and used without purification. IR spectra were recorded on a Perkin-Elmer FTIR Paragon 500. Combustion analyses were performed by the Analytical Lab, Marine Science Institute, University of California, Santa Barbara, CA 93106-6150.

2.2. *Synthesis of bis(2-amino-3-chloro-5-trifluoromethylpyridinium) tetrabromocuprate(II) (1)*

2-Amino-3-chloro-5-trifluoromethyl pyridine (TMCAP; 0.131 g, 0.67 mmol) was slurried in 1.0 mL of water. On addition of HBr (concentrated, 0.25 mL, excess), a colorless solution formed. A solution of $CuBr_2$ (0.074 g, 0.33 mmol) in 1.0 mL of water was added dropwise, slowly, to the stirring TMCAP solution and the resulting deep red–brown solution was filtered to remove any undissolved impurities. The solution had ether diffused into it. Black crystals, which X-ray analysis showed to be **1** $(TMCAPH)_2[CuBr_4]$, were isolated from the vial after 8 weeks. Yield: 0.1974 g (76.1%). CHN analysis; Calcd: C 18.59, H 1.29, N 7.20, found: C 18.8, H 1.24, N 7.16. IR (KBr) (cm^{-1}): 3281 (m, ν, $-NH_2$), 3247 (m, ν, $-NH_2$), 3171 (m), 1665 (s, δ, $-NH_2$), 1637 (s), 1452 (m), 1412 (m), 1366 (m), 1326 (s), 1280 (s), 1170 (s), 1132 (s), 1077 (m), 920 (w), 898 (s), 753 (m), 708 (m), 631 (m), 590 (m).

2.3. *Synthesis of bis(2-amino-3-chloro-5-trifluoromethylpyridinium) tetrachlorocuprate(II) (2)*

TMCAP (0.295 g, 1.5 mmol) was slurried in 2.0 mL of water. On addition of HCl (concentrated, 0.75 mL, excess), a colorless solution formed. A solution of $CuCl_2$ (0.128 g, 0.75 mmol) in 1.5 mL of water was added dropwise, slowly, to the stirring TMCAP solution and the resulting brilliant green solution was filtered to remove any undissolved impurities. The solution was placed in a crystallizing dish, left for slow evaporation at room temperature, and in 2 weeks brilliant lime green needle-like crystals of **2** formed. Yield: 0.2829 g (62.8%), CHN analysis; Calcd: C 24.00, H 1.68, N 9.33, found: C 24.00, H 1.62, N 9.23. IR (KBr) (cm^{-1}): 3324 (m, ν, $-NH_2$), 3194 (m, ν, $-NH_2$), 3155 (m), 1660 (s, δ, $-NH_2$), 1628 (s), 1442 (m), 1325 (s), 1278 (s), 1179 (m), 1135 (s), 1101 (m), 1076 (m), 901 (s), 708 (m), 633 (m).

2.4. *X-ray structure determination*

Single crystal X-ray diffraction (XRD) patterns for **2** were recorded at low temperature with a Rigaku-Spider curved image-plate detector using copper Kα radiation (Rigaku MM007 microfocus rotating anode generator), monochromated, and focused with high-flux Osmic multilayer mirror optics. Data were processed with FS Process (Rigaku (1998) [20]. PROCESS-AUTO: Automatic Data Acquisition and Processing Package for Imaging Plate and CCD Diffractometers, Rigaku Corporation, 3-9-12 Matsubara, Akishima, Tokyo 196-8666, Japan). Absorption correction: multi-scan [21].

Data for **1** were collected on a Bruker/Siemens Apex II diffractometer employing Mo-Kα radiation ($\lambda = 0.71073$ Å) with a graphite monochromator and using φ and ω scans for data collection at 150(2) K. Data collection, cell refinement, and data reduction were performed using SHELXTL [22]. Absorption corrections and data scaling were made *via* redundant data using SADABS [23].

Both structures were solved by direct methods and expanded *via* Fourier techniques [24]. All non-hydrogen atoms were refined anisotropically. Hydrogens bonded to nitrogen were located in the difference maps and their positions were refined using isotropic *U*-values. The aromatic hydrogens were refined *via* a riding model with fixed isotropic *U*-values. The structures of **1** and **2** have been deposited with the CCDC [25]. Full crystal and refinement details are given in table 1. Comparison of X-ray powder diffraction data with the crystallographic data of **1** and **2** established that the samples used for magnetic studies were of the same phase as the single crystals.

2.5. *Magnetic susceptibility*

Magnetic data were collected using a Quantum Design MPMS-XL SQUID magnetometer. The 0.1188 g powdered sample of **1** and the 0.0818 g powdered sample of **2** used in the magnetic studies were prepared from crushed single crystals. Samples were packed into small gelatin capsules and the magnetic moments were measured using magnetic fields of 0–50 kOe at 1.8 K. Several data points were collected as the magnetic field was brought back to 0 kOe to confirm that there was no hysteresis. Temperature-dependent magnetic susceptibility data were collected over a temperature range 1.85–310 K at an applied magnetic field of 1 kOe. Diamagetic corrections for the copper and halide ions were taken from Pascal's constants [1b]. These corrections and the temperature-independent paramagnetic (TIP) correction for the copper atom, $60 \times 10^{-6}\,\mathrm{cm^3\,mol^{-1}}$, were applied to the data sets. All data were interpreted with the Hamiltonian $H = -2J\Sigma\vec{S}_i \cdot \vec{S}_j$.

3. Results and discussion

3.1. *Analysis of crystal structures*

3.1.1. X-ray structure of *bis*(2-amino-3-chloro-5-trifluoromethylpyridinium)-tetrabromocuprate(II) (1). Compound **1** was obtained by reaction of solid $CuBr_2$ with two equivalents of 2-amino-3-chloro-5-trifluoromethylpyridine in acidic solution.

Table 1. Crystal data and structure refinement for **1** and **2**.

Compound	**1**	**2**
Empirical formula	$C_{12}H_{10}Br_4Cl_2CuF_6N_4$	$C_{12}H_{10}Cl_6Cu_1F_6N_4$
Formula weight	778.32	600.99
Temperature (K)	113(2)	123(2)
Wavelength (Å)	0.71073	1.5418
Crystal system	Monoclinic	Triclinic
Space group	$P2_1/c$	$P\bar{1}$
Unit cell dimensions (Å, °)		
a	6.9825(2)	8.3892(17)
b	21.0948(7)	21.640(4)
c	14.7271(5)	33.332(7)
α	90	82.32(3)
β	90.805(2)	89.99(3)
γ	90	85.00(3)
Volume (Å^3), Z	2169.01(12), 4	5974(2), 12
Calculated density (mg m^{-3})	2.383	2.005
Absorption coefficient (mm^{-1})	8.680	9.577
$F(000)$	1468	3546
Crystal size (mm^3)	$0.34 \times 0.12 \times 0.03$	$0.2 \times 0.02 \times 0.005$
Crystal color	Red	Lime green
θ range for data collection (°)	2.77–29.95	3.27–36.06
Limiting indices	$-9 \le h \le 9$; $-29 \le k \le 29$; $-20 \le l \le 20$	$-7 \le h \le 9$; $-26 \le k \le 26$; $-41 \le l \le 41$
Reflections collected	57,232	84,552
Independent reflections	6278 [R(int) = 0.0950]	21,842 [R(int) = 0.1023]
Completeness	To 0.595 Å^{-1} 99.9%	To 0.599 Å^{-1} 95.7%
Absorption correction	Multi-scan	Multi-scan
Refinement method	Full-matrix least-squares on F^2	Full-matrix least-squares on F^2
Data/restraints/parameters	6278/0/280	21,842/240/1680
Goodness-of-fit on F^2	1.009	0.973
Final R indices [$I > 2\sigma(I)$]	$R_1 = 0.0362$, $wR_2 = 0.0552$	$R_1 = 0.1043$, $wR_2 = 0.2574$
R indices (all data)	$R_1 = 0.0724$, $wR_2 = 0.0641$	$R_1 = 0.1742$, $wR_2 = 0.3302$
Largest difference peak and hole (e Å^{-3})	0.619 and −0.668	2.104 and −1.733

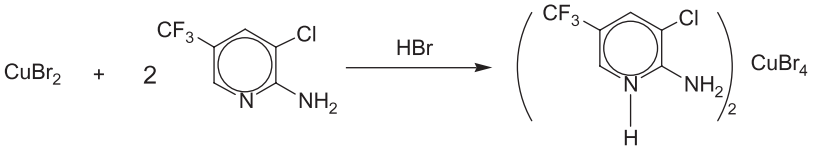

Figure 2. Synthesis of $(TMCAP)_2[CuBr]_4$ (**1**).

Red crystals of **1** were obtained by ether diffusion into a portion of the reaction solution. The synthesis is shown in figure 2.

Compound **1** crystallizes in the monoclinic space group $P2_1/c$. The asymmetric unit of **1** is shown in figure 3. The structural unit consists of one $CuBr_4^{2-}$ and two 2-amino-3-chloro-5-trifluoromethylpyridinium ions. The $CuBr_4^{2-}$ forms a distorted tetrahedron with a mean *trans* angle of 130°, the large Br1–Cu–Br4 angle being 133.89(2)° and Br2–Cu–Br3 125.85(2)°. The copper bromide bond lengths, averaging 2.378 Å, are in the normal range [8].

The aminopyridinium cations are almost planar with root mean square (RMS) deviations of 0.0084 Å and 0.0076 Å from the plane in the N1 and N11 rings, respectively.

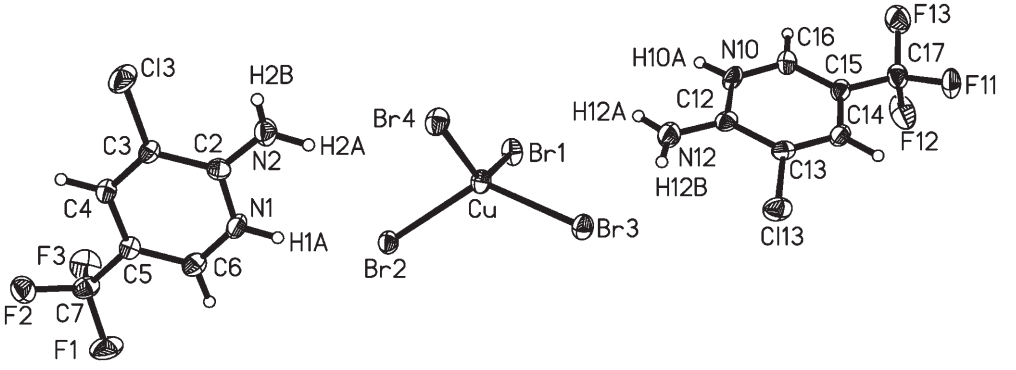

Figure 3. The asymmetric unit of **1** showing 50% probability ellipsoids. Only those hydrogen atoms for which the positions were refined are labeled. Selected bond lengths and angles for **1** are shown in table S1 (Supplementary material).

The amino, chloro, and carbons of the trifluoromethyl carbon substituents are almost co-planar with the rings with the chlorines bent slightly (−0.087 Å) to the opposite side of the plane relative to the other two substituents (0.037 for NH_2, 0.092 for CF_3). The planes of the amino groups (N1, H2A, H2B and N12, H12A, H12B) are rotated 3.6° and 1.9° relative to the pyridinium rings. The two cations are canted 74.1° to each other.

The packing of $CuBr_4^{2-}$ in the crystal forms a complex network *via* short Br···Br contacts. The $CuBr_4^{2-}$ anions form ladders parallel to the *bc* face (figure 4). In the ladder, the closest non-bonding contact Br1–Br1A (d_1), related by inversion, has a distance of 3.526 Å. This is a very short contact compared to most other $CuBr_4^{2-}$ anions in A_2CuBr_4 systems [8]. Together with a favorable torsion angle of 180° (Cu–Br1···Br1A–CuA), this contact should be significant in propagating antiferromagnetic interactions. The next closest interaction, Br1A···Br2B (d_2), is 4.009 Å and the third closest distance, Br1···Br2B (d_3), is 4.069 Å. The $CuBr_4^{2-}$ ladders may be formed *via* close contacts in two different ways. In one option, the short contact d_1 forms the rungs of the ladder while d_2 forms the rails. In the second option, the double contact d_3 forms the rungs and d_2 still forms the rails. In either case, the contact d_1 or d_3, whichever is not viewed as the rung interaction, introduces a diagonal term to the lattice. In considering which of these is the rung, d_1 is the shortest whereas d_3 forms double contacts, and so both must be considered as potentially contributing magnetic pathways within the ladder. All Br···Br contact data are summarized in table 2.

The $CuBr_4^{2-}$ anions also form linear chains parallel to the *c*-axis (figure 5). The separation between each successive bromide is 4.076 Å and is the longest Br···Br non-bonding contact. In fact, this fourth interaction from one ladder to the next cannot be ignored. This distance, for example from Br4 to the closest bromine (Br3) in the next ladder, 4.076 Å, is not much longer than d_3. When all four contacts are considered, the $CuBr_4^{2-}$ anions form a very well-isolated double layer with complex interactions within the layers. The $CuBr_4^{2-}$ ions zigzag within these.

The cations are inserted between $CuBr_4^{2-}$ layers and there are close contacts between the chloro groups on the pyridinium rings and bromides of $CuBr_4^{2-}$ ($d_{Br2}\cdots_{Cl3}$, 3.510 Å; $d_{Br4}\cdots_{Cl3}$, 3.767 Å; and $d_{Br4}\cdots_{Cl13}$, 3.705 Å; figure 6). A fluorine···fluorine close contact

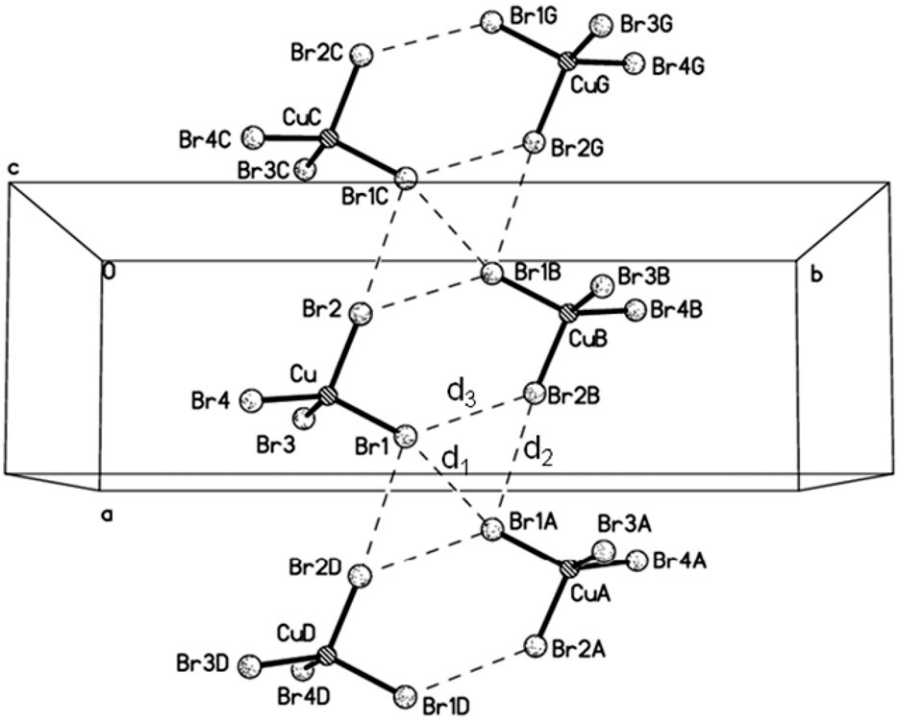

Figure 4. Ladders of $CuBr_4^{2-}$ anions in **1** are formed by short non-bonding Br···Br contacts (dashed lines). d_1, 3.526 Å (Br1···Br1A); d_2, 4.009 Å (Br1A···Br2B); and d_3, 4.069 Å (Br1···Br2B).

Table 2. Br···Br contact parameters for the $CuBr_4^{2-}$ ions in **1**.

Contacts	$d_{(Br\cdots Br)}$ (Å)	θ_1	θ_2	τ
Br1···Br1A	$d_1 = 3.526$	156.9(1)	156.9(1)	180
Br1A···Br2B	$d_2 = 4.009$	151.5(1)	99.8(1)	81.7(1)
Br1···Br2B	$d_3 = 4.069$	118.6(1)	129.0(1)	55.8(1)
Br3···Br4F	$d_4 = 4.076$	143.3(1)	164.6(1)	88.3(6)

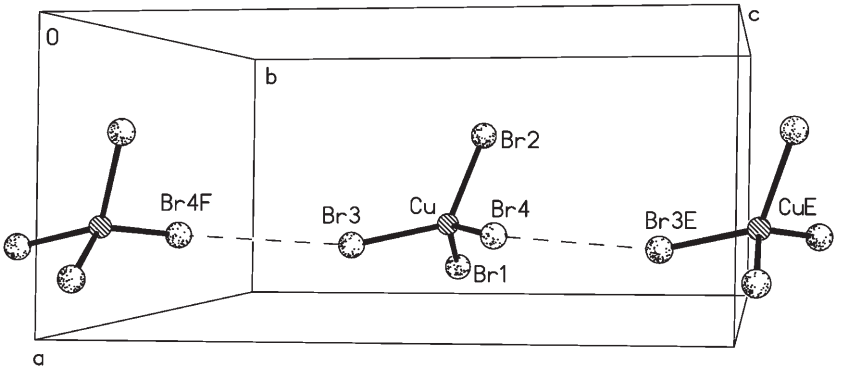

Figure 5. Linear chains of the $CuBr_4^{2-}$ anions in **1** with dashed lines indicating the Br···Br close contacts.

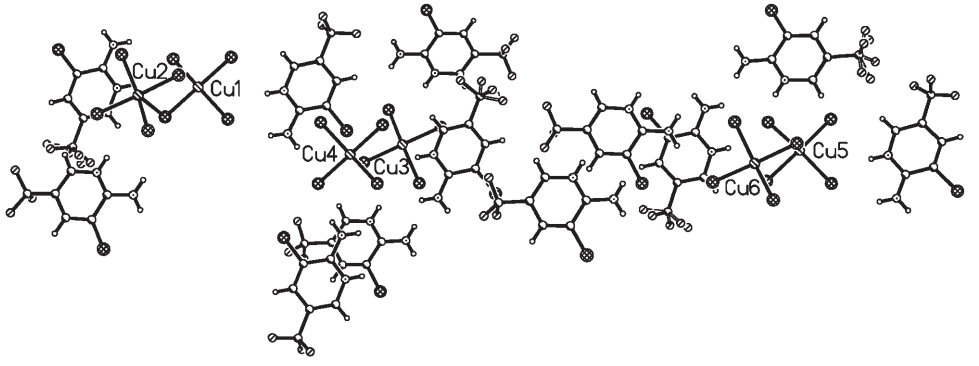

Figure 6. The asymmetric unit of **2**. Only the six Cu ions are labeled for clarity.

is also found between atoms in one pyridinium cation and a neighboring cation with the F1···F12 (symmetry $x+1$, $y+1$, $z+1$) distance being 2.967 Å. The structure is further stabilized by significant hydrogen bonding from both of the pyridinium hydrogens to bromide (table S2).

3.1.2. X-ray structure of *bis*(2-amino-3-chloro-5-trifluoromethylpyridinium)-tetrachlorocuprate(II) (2). Compound **2** was obtained by reaction of solid $CuCl_2$ with two equivalents of 2-amino-3-chloro-5-trifluoromethylpyridine in acidic solution. Lime green crystals of **2** were obtained by slow evaporation of the reaction solution over a period of 2 weeks. Compound **2** crystallizes in the triclinic space group $P\bar{1}$ with 18 independent ions in the unit cell (figure 6), 12 2-amino-3-chloro-5-trifluoromethylpyridinium cations, and six $CuCl_4^{2-}$ anions.

The pyridinium cations show bond lengths and angles similar to those observed for **1**. Complete bond lengths and angles may be found in the "Supplementary material." Two-site disorder was observed for the CF_3 groups of four cations (the D, H, J, and K rings) and modeled as such in the final crystallographic refinement. The pyridinium cations are nearly planar (table S3) with the largest RMS deviation from the plane being 0.0128 Å. All amino groups are planar, but rotated slightly (from 0.2° to 4.5°, table S3), with respect to the pyridinium rings. Similarly, the chlorines are slightly out of the plane of the pyridinium rings with five being above and seven below the plane with respect to the amino groups (table S3). These displacements are very similar to those seen in **1**.

The $CuCl_4^{2-}$ ions are nearly square planar with mean *trans* angles of: Cu1 171.99(12)°, Cu2 168.08(10)°, Cu3 171.87(1)°, Cu4 171.73(10)°, Cu5 165.68(1)°, and Cu6 168.69(10)° (figure 7). Each $CuCl_4^{2-}$ is associated with a second to create dimeric structures *via* bridging Cl ions. Each dimer is subtly different. The Cu1/Cu2 dimer is monobridged with a short weak coordinative bond of 2.763(3) Å between Cu2 and Cl13 and a longer one of 2.806(3) Å between Cu1 and Cl23; in the Cu3/Cu4 dimer, there are longer semi-coordinate bonds between each copper ion and a chloride in the neighboring $CuCl_4^{2-}$ (Cu3 to Cl43 is 2.854(3) Å and Cu4 to Cl33 is 2.839(3) Å) and the Cu5/Cu6 dimer has two short semi-coordinate bonds (Cu5···Cl63 2.741(3) Å; Cu6···Cl53 2.715(3) Å).

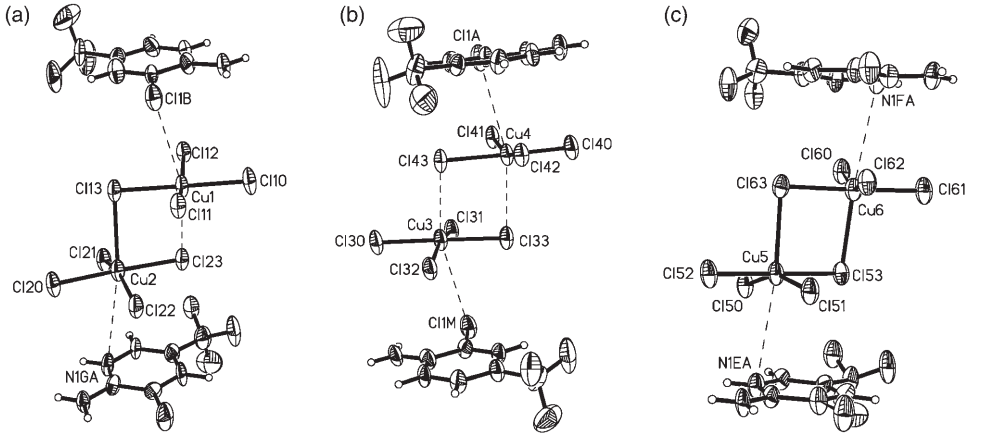

Figure 7. The (a) Cu1/Cu2, (b) Cu3/Cu4, and (c) Cu5/Cu6 dimers in **2** showing 50% probability ellipsoids. Dashed lines show the closest distances between each Cu ion and its nearest neighboring atoms.

In each case, the uncoordinated site, which would complete an octahedral environment about copper, is blocked by a TMCAPH cation but with different atoms lying closest to the Cu ions making each $CuCl_4^{2-}$ dimer distinct in its stereochemistry and packing within the crystal. In the Cu1/Cu2 dimer, the potential sixth coordination site on one Cu ion is blocked by a chlorine (Cu1···Cl1B 3.327 Å), whereas the other is closest to a pyridinium nitrogen (Cu2···N1GA = 3.563 Å; figure 7). For the Cu3/Cu4 dimer (figure 7), both copper ions of the dimer are associated with chlorines in adjacent cations. Cu3 interacts with Cl1B at a distance of 3.377 Å and Cu4 with Cl1A at 3.398 Å. In the third dimer (figure 7), both copper ions are associated with pyridine nitrogens, Cu5···N1EA (3.521 Å) and Cu6···N1FA (3.530 Å), in neighboring cations.

There is an interesting and subtle effect that shorter (<2.76 Å) semi-coordinate Cu···Cl interactions are *trans* to the weakly interacting pyridinium nitrogens on the TMCAPH cation, whereas the longer (>2.81 Å) semi-coordinate Cu···Cl interactions are *trans* to the quite closely associated chloro group on the TMCAPH cation. The shorter semi-coordinate bonds are also associated with less obtuse Cl–Cu–Cl bond distances (<159° compared to >164°) for the *trans*-related pair of Cl ions not involved in the dimeric association.

These dimers form ladders parallel to the *a*-axis *via* short Cl···Cl contacts (figure 8). All Cl···Cl contact data are summarized in table 3. Due to the presence of six different $CuCl_4^{2-}$ ions in the asymmetric unit, the dimers stack to make three crystallographically unique ladders with each having two different rail interactions (parallel to the *b*-axis). The rungs of the ladders are the dimers and the rails are formed by short Cl···Cl contacts between the dimers.

Each $CuCl_4^{2-}$ is hydrogen bonded to two pyridinium cations (figure 9). The hydrogen bonding to Cu3 is shown as an example. Cl30 is hydrogen bonded to the pyridinium hydrogen H1BA, and Cl32 is hydrogen bonded to H2BA of the amino substituent. It is likely that H1BA is involved in a bifurcated hydrogen bond with Cl32 as is the case for H1IA (see below), but the distance is slightly outside the cutoff value of 3 Å. The pyridinium hydrogen, H1IA, forms a bifurcated bond with both Cl33 and Cl31, with

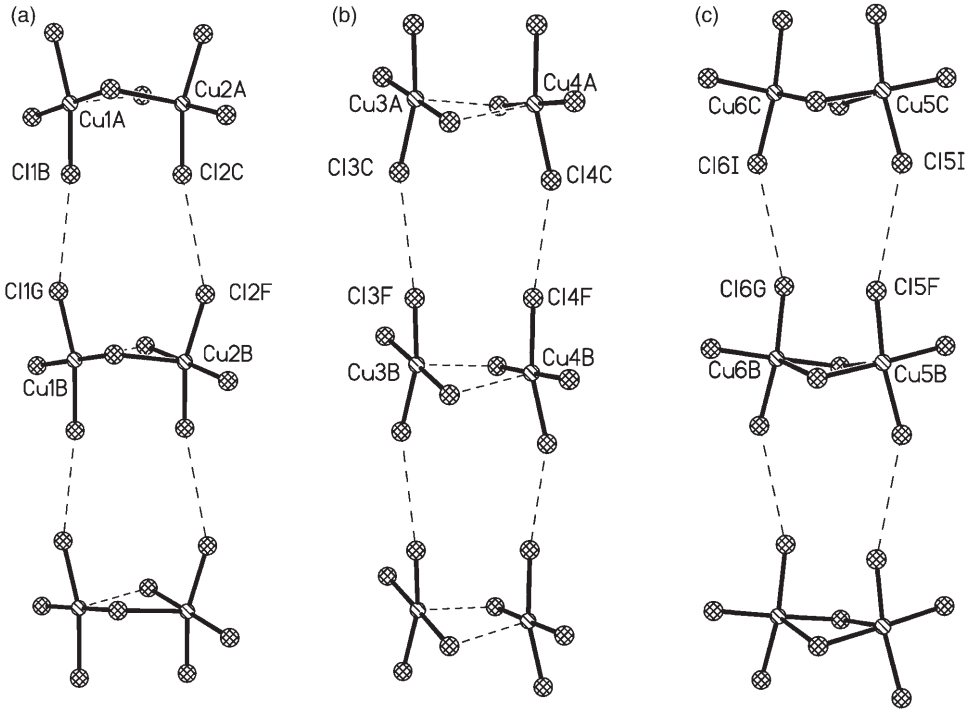

Figure 8. The (a) Cu1/Cu2, (b) Cu3/Cu4, and (c) Cu5/Cu6 ladders of **2**. Dashed lines show long (>2.81 Å) semi-coordinate Cu···Cl interactions within the dimers and Cl···Cl contacts.

Table 3. Cl···Cl contact parameters for the $CuCl_4^{2-}$ ladders in **2**.

Contacts	d(Cl···Cl) (Å)	θ_1	θ_2	τ
Cl1B···Cl1G	3.911	158.0	159.6	138.9
Cl2C···Cl2F	3.989	157.4	151.9	130.3
Cl3C···Cl3F	3.910	156.5	156.5	−138.9
Cl4C···Cl4F	3.909	159.0	156.5	−138.9
Cl5I···Cl5F	3.988	153.3	158.6	125.0
Cl6I···Cl6G	3.983	152.4	159.4	−131.0

the latter also associated with the amino hydrogen H2IA. Representative hydrogen bond parameters are given in table 4.

In addition, stacked $Cu_2Cl_8^{4-}$ units are stabilized and linked into chains parallel to the *a*-axis by hydrogen bonding. Figure 10 shows the details of a portion of one such chain (the Cu5 chain). In the chains, each pyridinium cation is associated with two $CuCl_4^{2-}$ anions *via* hydrogen bonding. The pyridinium hydrogen H1EA forms a bifurcated bond with two chlorides (Cl52 and Cl50) in the neighboring $CuCl_4^{2-}$. Cl50 also forms a hydrogen bond with one of the amino group hydrogens (H2EA) in the same cation, while the other amino group hydrogen (H2EB) is hydrogen bonded to a chloride ion (Cl5C) in the next $CuCl_4^{2-}$ of the chain. Representative hydrogen bond parameters are given in table 4.

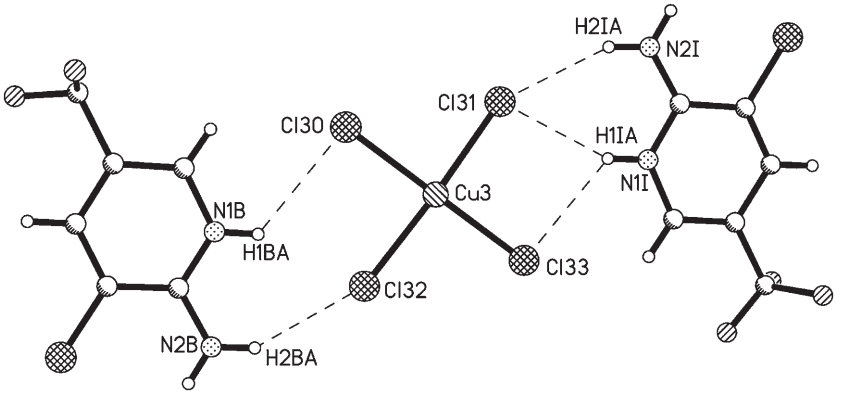

Figure 9. Hydrogen bonding between a $CuCl_4^{2-}$ anion and two pyridinium ions in **2**.

Table 4. A representative set of hydrogen bonds for **2** (Å and °).

D–H···A	*d*(H···A)	*d*(D···A)	∠(DHA)
N1B–H1BA···Cl30	2.75	3.324(9)	125.4
N2B–H2BA···Cl32	2.51	3.281(8)	149.1
N1I–H1IA···Cl33	2.69	3.298(9)	128.6
N1I–H1IA···Cl31	2.50	3.286(8)	153.0
N1E–H1EA···Cl50	2.38	3.190(8)	156.1
N1E–H1EA···Cl52	2.86	3.388(9)	121.6
N2E–H2EA···Cl50	2.56	3.314(8)	147.2
N2E–H2EB···Cl5C	2.50	3.330(9)	159.6

These contacts are illustrated in figures 9 and 10.

3.2. *Magnetic properties of 1 and 2*

Magnetization data of **1** as a function of temperature are plotted as χ *versus* T in figure 11. A maximum of $\chi_{mol} = 4.03 \times 10^{-3}$ emu (mol Oe)$^{-1}$ near 45 K is observed and clearly indicates the presence of a significant antiferromagnetic interaction. The molar susceptibility decreases as the temperature decreases until a minimum near 6 K is obtained. Below that temperature, the molar susceptibility increases again, suggesting the presence of a paramagnetic impurity.

The antiferromagnetic properties of **1** are also reflected in the χT *versus* T plot, which shows a downward curvature with decreasing temperature (figure 11). At high temperature, the value of χT is still rising as a result of moderately strong interactions. A variety of known models were used to fit the experimental magnetic data. The best fit was obtained when using a strong-rung ladder model [26], which is shown by the solid line in figure 11, giving $C = 0.4289(8)$, $2J_{rung} = -55.91(8)$, and $2J_{rail} = -43.18(18)$ K with a small amount of paramagnetic impurity $P = 0.975\%$.

The connectivity of the $CuBr_4^{2-}$ ions in **1** is a ladder, with a diagonal term, if only the three shortest contacts are considered. The strong interaction may be explained by the short non-bonding Br···Br distance of 3.526 Å. Strong antiferromagnetic interactions have been reported in other compounds with similar short distances [27]. Given the

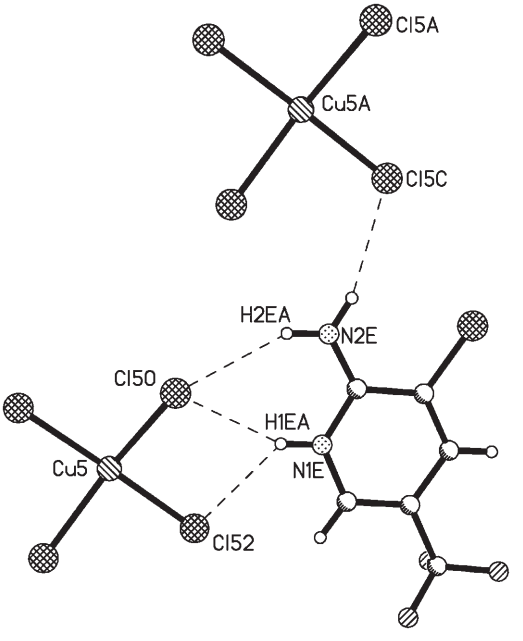

Figure 10. A portion of the Cu5 chain in **2**.

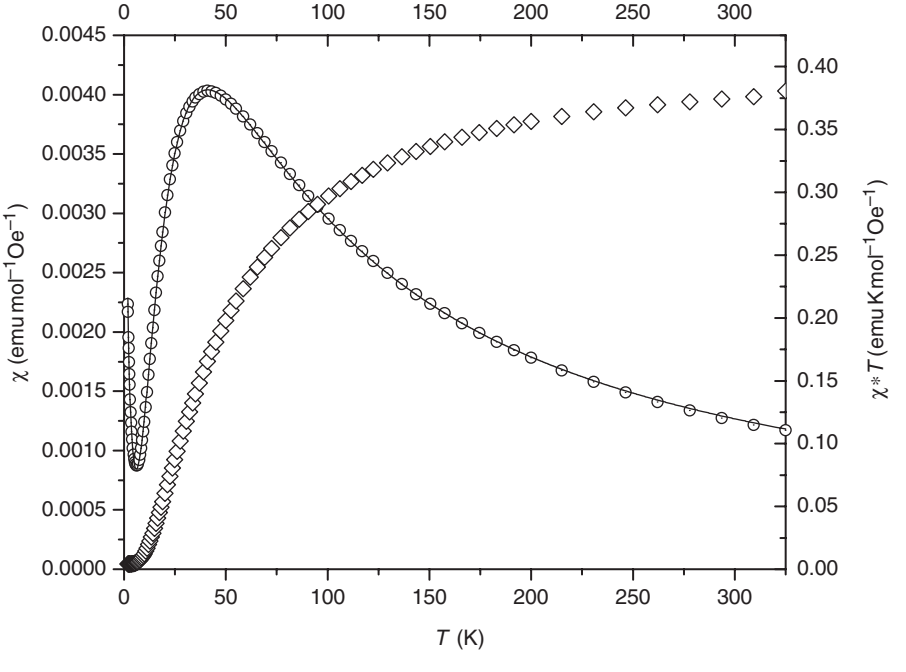

Figure 11. Plot of χ_{mol} *vs.* T (open circle) and χT *vs.* T (open diamond) for **1**. The solid line is the fit to the magnetic ladder, strong-rung model.

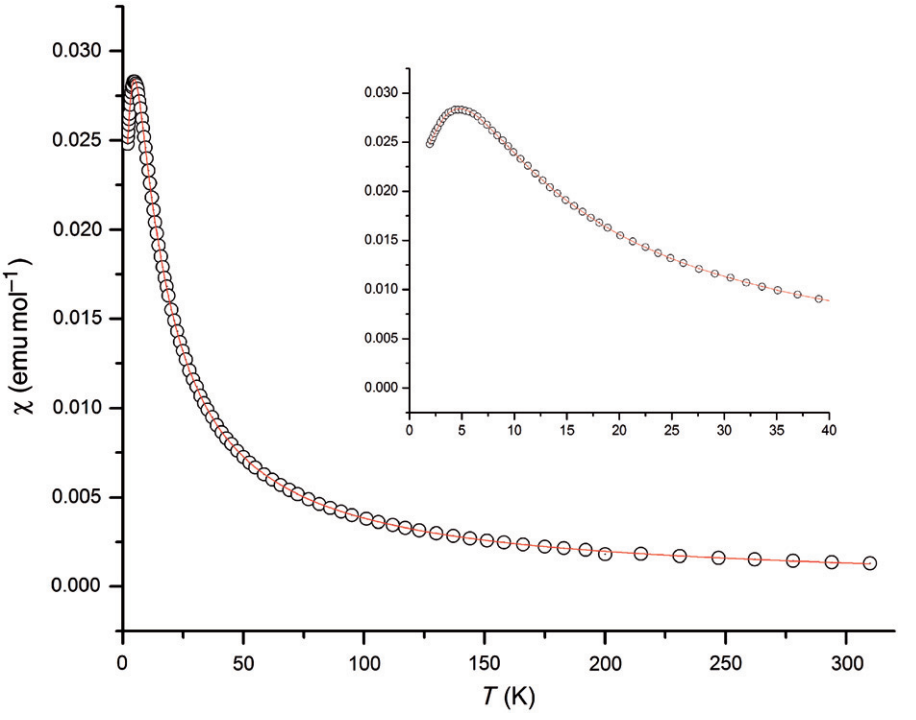

Figure 12. Plot of χ_{mol} *vs.* T (open circle) **2**. The solid line is the fit to the magnetic ladder, strong-rail model.

Br···Br contact geometry shown in table 3, and the observation that the double halide exchange tends to be strongest for shorter values of d, large values of θ, and values of τ near 0° or 180°, we can estimate which interactions should be the most significant. Distance d_1 should clearly mediate the strongest interaction. The three remaining contacts have similar Br···Br distances, but none show optimum angles. Distance d_4 shows fairly large θ values, but τ is nearly 90° as is the case for d_2. Distance d_3 is more promising with a smaller τ angle, but both θ values are significantly less than those of d_4. In addition, the observation that the data can fit well only by the strong-rung ladder model does not, *a priori*, indicate that the compound is a magnetic ladder, as has been demonstrated previously [12]. It is clear from the data that the material has a singlet ground state, but beyond that one cannot say with certainty the magnetic interaction pathways.

The molar susceptibility of **2** was collected as a function of temperature between 1.80 and 310 K (figure 12). A maximum of $\chi_{mol} = 4.02 \times 10^{-3}$ emu (mol Oe)$^{-1}$ near 5 K is observed in the graph of χ *versus* T, indicating a weak antiferromagnetic interaction. The data were fit to an antiferromagnetic strong-rail ladder model [15]. Attempts to fit the data to other models including a dimer and a strong-rung ladder resulted in poor fits and unphysical parameters, such as negative percent impurities. The strong-rail model gave a Curie constant of 0.402(1) with $2J_{rung} = -4.02(7)$ K, $2J_{rail} = -7.946(9)$ K, and $R^2 = 0.99999$. A strong-rail ladder is the most unusual with only two being reported previously [15, 28]. Although this is the best fit, we recognize that **2** is not a true ladder; examination of the structure shows that this is an approximation at best. Within each

ladder, there are two different rail exchange constants. The analytical model assumes that the exchange *via* the two rail pathways are the same, so even within one ladder the use of this exchange model is not strictly valid. Additionally, there are three distinct ladders in the structure leading to nine different exchange constants. Thus, the fitted values from the bulk data provide an average value for the three ladders. (The expanded curve from 1.95 to 40 K in the inset of figure 12 demonstrates the good fit near the maximum in χ.)

Exchange within the dimers (the rungs of the ladders) occurs *via* semi-coordinate Cu–Cl bonds averaging 2.80 ± 0.06 Å with similar bridging angles making it reasonable to assume that the exchange constants across the rungs are similar between the ladders and the average value given from the fit is a good measure for each ladder. Similarly, the contact parameters for the ladder rails (table S4) also support the idea that although the fitted exchange values must represent an average, each rail exchange is likely to be very close to that average. Moreover, the narrow range of Cl···Cl contact distances (3.8–4.0 Å), of Cu–Cl···Cl angles (151.9–159.6°) and of Cu–Cl···Cl–Cu torsion angles (absolute value 125–138.9°) and variable stereochemistry of the $Cu_2Cl_8^{4-}$ dimers are consistent with the very small estimated standard deviation associated with $2J_{rail}$ compared to $2J_{rung}$.

4. Conclusions

The bis(2-amino-3-chloro-5-trifluoromethylpyridinium)tetrabromocuprate(II) and bis(2-amino-3-chloro-5-trifluoromethylpyridinium)tetrachlorocuprate(II) are packed very differently into their crystalline forms. Both exhibit antiferromagnetic coupling with significant interactions, best fit to a strong-rung ladder model, being found in the bromo compound and weak interactions, best fit to a strong-rail ladder model, being found for the chloro compound. The structures of the compounds show that although the magnetic data may be fit to the respective ladder models, the values obtained (**1**, $2J/k_B \sim 50$ K and **2**, $2J/k_B \sim 6$ K) are only approximate or average values. Theoretical calculations will be required to determine the specific nature of the magnetic lattices.

The magnetic interactions observed along the rails of **2** can be compared to the value obtained for a similar interaction in the chain structure of bis(2-amino-3-chloropyridinium)tetrachlorocuprate [3], where the $CuCl_4^{2-}$ ions interact *via* chloride···chloride contacts. The value of −1.3 K reported is substantially weaker than that observed in **2** (approximately −8 K), which is not at all surprising given the Cl···Cl separations of ~4.59 Å compared to ~3.91–3.99 Å for **2**. Although there are no reported structures which can serve as models for the overall packing of the $CuCl_4$ bichloride-bridged dimers as ladders *via* short chloride···chloride contacts, one can compare the magnetic interactions of the bichloride bridged dimers to known species. For example, the 1,10-phenanthrolinedione dichlorocopper complex reported by Kou *et al*. [29] exhibits the same type of bichloride linkage between the Cu ions. The authors report magnetic exchange through the bichloride bridge of $2J/k_B = -0.83$ K/-0.55 cm^{-1}, a factor of four weaker than the rung interactions in **2**. This significantly weaker interaction might be surprising in light of the shorter Cu–Cl distances in this bridge (2.26 Å, 2.69 Å) relative to **2** (2.25–2.34 Å, 2.71–2.84 Å). However, it simply lends

support to the theory that such magnetic exchange is dependent upon bridging and dihedral angles in the superexchange pathway as much as the interatomic distances.

Acknowledgments

Funding for the powder X-ray diffractometer and SQUID magnetometer was provided by the Kresge Foundation, PolyCarbon Industries Inc. and the National Science Foundation. Funding for the Rigaku diffractometer was provided by the MacDiarmid Institute for Advanced Materials and Nanotechnology. JLW is grateful to the University of Canterbury for sabbatical leave.

References

[1] (a) R.H. White. *Quantum Theory of Magnetism*, 2nd Edn, Springer-Verlag, Berlin (1983); (b) R.L. Carlin, *Magnetochemistry*, Springer-Verlag, Berlin (1986); (c) O. Kahn, *Molecular Magnetism*, VCH Publishers, New York (1993); (d) L.J. Longh (Ed.). *Magnetic Properties of Layered Transition Metal Compounds*, Kluwer Academic Publishers, Dordrecht (1990).
[2] W.E. Marsh, E.J. Valence, D.J. Hodgson. *Inorg. Chim. Acta*, **51**, 49 (1981).
[3] S.N. Herringer, M.M. Turnbull, C.P. Landee, J.L. Wikaira. *J. Coord. Chem.*, **62**, 863 (2009).
[4] R.J. Butcher, J.J. Novoa, J. Ribas-Ariño, A.W. Sandvik, M.M. Turnbull, C.P. Landee, B.M. Wells, F.F. Awwadi. *Chem. Commun.*, **18**, 1359 (2009).
[5] (a) K. Halvorson, R.D. Willett. *Acta Crystallogr., Sect. C: Cryst. Struct. Commun.*, **44**, 2071 (1988); (b) G.V. Rubenacker, J.E. Drumheller. *J. Magn. Magn. Mater.*, **79**, 119 (1989); (c) P. Zhou, J.E. Drumheller. *J. Appl. Phys.*, **67**, 5755 (1990).
[6] H. Place, R.D. Willett. *Acta Crystallogr., Sect. C: Cryst. Struct. Commun.*, **43**, 1050 (1987).
[7] (a) T. Manfredini, G.C. Pellacini, A. Bonamartini-Corradi, L.P. Battaglia, G.G.T. Gaurini, J.G. Guisti, R.D. Willett, D.X. West. *Inorg. Chem.*, **29**, 221 (1990); (b) C. Zanchini, R.D. Willett. *Inorg. Chem.*, **29**, 3027 (1990).
[8] M.M. Turnbull, C.P. Landee, B.M. Wells. *Coord. Chem. Rev.*, **249**, 2567 (2005).
[9] G.M. Espallargas, L. Brammer, J. vande Streek, K. Shankland, A.J. Florence, H. Adams. *J. Am. Chem. Soc.*, **128**, 9584 (2006).
[10] B. Jasiewicz, W. Boczon, D. Muth, B. Warzajtis, U. Rychlewska, B. Andrzejewski, T. Tolinski. *J. Mol. Struct.*, **794**, 311 (2006).
[11] F.F. Awwadi, R.D. Willett, B. Twamley. *Cryst. Growth Des.*, **7**, 624 (2007).
[12] L. Li, M.M. Turnbull, C.P. Landee, J. Jornet, M. Deumal, J.J. Novoa, J.L. Wikaira. *Inorg. Chem.*, **46**, 11254 (2007).
[13] C. Zhong, T. Sasaki, A. Jimbo-Kobayashi, E. Fujiwara, A. Kobayashi, M. Tada, Y. Iwasawa. *Bull. Chem. Soc. Japan*, **80**, 2365 (2007).
[14] S.S. Staniland, A. Harrison, N. Robertson, K.V. Kamenev, S. Parsons. *Inorg. Chem.*, **45**, 5767 (2006).
[15] A. Shapiro, C.P. Landee, M.M. Turnbull, J. Jornet, M. Deumal, J.J. Novoa, M.A. Robb, W. Lewis. *J. Am. Chem. Soc.*, **129**, 952 (2007).
[16] S.F. Haddad, R.H. Al-Far. *J. Chem. Crystallogr.*, **38**, 663 (2008).
[17] C.J. Adams, M.A. Kurawa, M. Lusi, A.G. Orpen. *CrystEngComm.*, **10**, 1790 (2008).
[18] J. Bai, G. Wang, L. Zhang, C. Wang, Y.-H. Huang, D.-C. Fang, Q. Li. *Gaodeng Xuexiao Huaxue Xuebao* (*Chem. J. Chin. Univ.,* Chinese Edition), **28**, 1113 (2007).
[19] (a) F.M. Woodward, A.S. Albrecht, C.M. Wynn, C.P. Landee, M.M. Turnbull. *Phys. Rev. B*, **65**, 144412 (2002); (b) C.P. Landee, M.M. Turnbull, C. Galeriu, J. Giantsidis, F.M. Woodward. *Phys. Rev. B: Rapid Commun.*, **63**, 100402R (2001); (c) F.M. Woodward, C.P. Landee, J. Giantsidis, M.M. Turnbull, C. Richardson. *Inorg. Chim. Acta*, **324**, 324 (2001); (d) T.J. Coffey, C.P. Landee, W.T. Robinson, M.M. Turnbull, M. Winn, F.M. Woodward. *Inorg. Chim. Acta*, **303**, 54 (2001).
[20] Rigaku. *PROCESS-AUTO*, Rigaku Corporation, Tokyo, Japan (1998).
[21] T. Higashi. *ABSCOR*, Rigaku Corporation, Tokyo, Japan (1995).
[22] G.M. Sheldrick. *SHELXTL: Version 5.10, Structure Determination Software Suite*, Bruker AXS Inc., Madison, WI (2001).

[23] G.M. Sheldrick. *SADABS*, *Program for Empirical Absorption Correction of Area Detector Data*, University of Göttingen, Germany (1996).
[24] G.M. Sheldrick. *SHELX97-2*, *Programs for the Solution and Refinement of Crystal Structures*, University of Göttingen, Germany (1997).
[25] CCDC 761101 (**1**) and CCDC 761100 (**2**). This contains the supplementary crystallographic data for this article, these data can be obtained free of charge from The Cambridge Crystallographic Data Centre via www.ccdc.cam.ac.uk/data_request/ci.
[26] D.C. Johnston, M. Troyer, S. Miyahara, D. Lidsky, K. Ueda, M. Azuma, Z. Hiroi, M. Takano, M. Isobe, Y. Ueda, M.A. Korotin, V.I. Anisimov, A.V. Mahajan, L.L. Miller, arXiv:cond-mat/0001147 (2000).
[27] (a) R.D. Willett, M. Middleton. *J. Am. Chem. Soc.*, **110**, 8639 (1998); (b) R.D. Willett, K. Halvorson. *Acta Crystallogr. C: Cryst. Struct. Commun.*, **44**, 2071 (1988); (c) G.V. Rubenacker, S. Waplak, S.L. Hutton, D.N. Haines, J.E. Drumheller. *J. Appl. Phys.*, **57**, 3341 (1985); (d) L.O. Snively, D.N. Haines, K. Emerson, J.E. Drumheller. *Phys. Rev. B: Condens. Matter*, **26**, 5245 (1982); (e) N. Sivron, T.E. Grigereit, J.E. Drumheller, K. Emerson, R.D. Willett. *J. Appl. Phys.*, **75**, 5952 (1994).
[28] R.D. Willett, C. Galeriu, C.P. Landee, M.M. Turnbull, B. Twamley. *Inorg. Chem.*, **43**, 3804 (2004).
[29] Y.-Y. Kou, J.-L. Tian, D.-D. Li, H. Liu, W. Gu, S.-P. Yan. *J. Coord. Chem.*, **62**, 2182 (2009).